# A Single-Stage DC Fast Charger with Enhanced Reactive Power Compensation Capability

Avinash Dornala
*Student Member*, *IEEE*
Elmore Family School of Electrical and Computer Engineering, Purdue University
West Lafayette, USA
adornal@purdue.edu

Woongkul Lee
*Senior Member*, *IEEE*
Elmore Family School of Electrical and Computer Engineering, Purdue University
West Lafayette, USA
wklee@purdue.edu

***Abstract*—A single-stage indirect matrix converter (SSIMC) has emerged as a promising solution for DC fast chargers (DCFC) and front-end rectifiers, offering galvanic isolation with high frequency transformer, high power density, and improved efficiency compared with conventional two-stage converters. Numerous studies suggest SSIMC as a potential DCFC application. However, the existing SSIMC-based DCFC systems are mainly studied for unity power factor operation with optimized modulation methods to reduce transformer RMS current. The variation of transformer voltage and RMS current with grid side power factor is not yet fully investigated. To address this gap, this paper analyzes the SSIMC, providing the variation of transformer primary voltage and the RMS current with the grid side power factor. Based on the results obtained, a DCFC operation methodology is proposed with two modes of operation. mode-I is defined with the battery in place while charging, and mode-II is where the SSIMC is idle with the output capacitor. It is shown that the DCFC system operates with reactive power support up to converter limits to the grid during mode-II operation, utilizing the output capacitor.**

***Index Terms*—DC fast charging, EV charging, matrix converters, reactive power control, vehicle-to-grid**

## I. Introduction

Efficient vehicle-to-grid (V2G) systems are in demand for the rapidly increasing electric vehicles (EVs), providing additional ancillary services to the grid. A single-stage indirect matrix converter (SSIMC), with the elimination of intermediate energy storage and isolation, offers an efficient, high-power-density solution for DC fast charger (DCFC) applications. The SSIMC, as shown in Fig. 1, is well studied in the literature [1]-[3] for G2V/V2G applications for bidirectional power transfer capability. However, the current SSIMC systems studies are mainly focused on unity power factor operation, focusing on reduced transformer RMS current. A detailed quantitative study of the variation of transformer RMS current at other operating conditions needs to be evaluated. Hence, to address this gap, this paper provides an analytical study of the SSIMC, providing the variation of transformer current, grid active and reactive power with grid-side power factor. Based on the obtained results, the SSIMC system with two modes of operation is defined. Mode-I is defined with the battery in place while charging, and mode-II is where the SSIMC is idle with the output capacitor. It is shown that the SSIMC can be utilized for

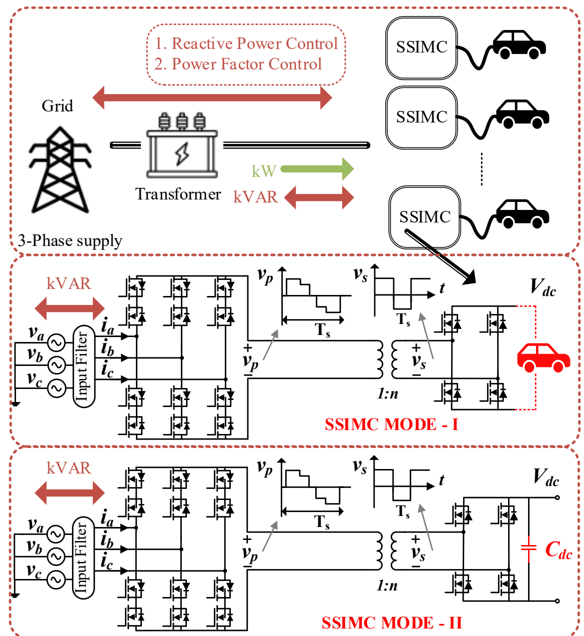


Fig. 1. Typical SSIMC topology in a DC fast charger application, with V2G functionalities, highlighting mode-I and mode-II operation.

reactive power compensation at converter limits in the mode-II operation.

The EV charger for reactive power compensation is extensively studied in the literature, showing its decoupled power control capability [3] in the case of single-phase two-stage converters. Accordingly, several topologies are investigated [4] for reactive power support considering level-1 and level-2 operation. Further, Recent studies [5] indicate that constant-voltage control at the DC capacitor improves reactive power compensation, where the design of the output capacitor and voltage control are investigated. The capacitor voltage control methodology is shown to achieve a lower power rating of the EV charger as discussed in [6]. Concerning the three-phase off-board chargers, the SSIMC-based DCFC is proposed in [7], showing its operation for V2G/G2V modes. Several modulation methods of SSIMC [8], [9], [10], [11] are proposed for unity power factor operation, focusing on reduced transformer RMS current and overall efficiency. The SSIMC operation with decoupled power control is investigated in [12],

XXX-X-XXXX-XXXX-X/XX/$XX.00 ©20XX IEEE
979-8-3315-8138-1

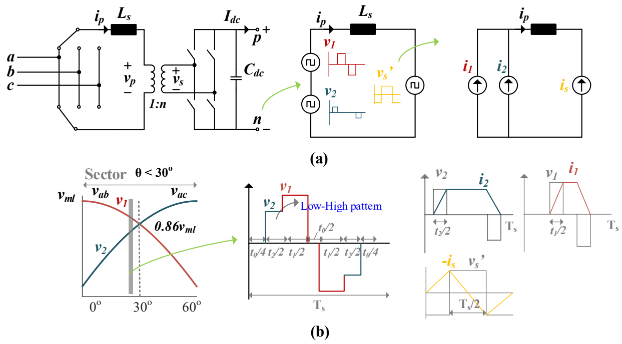


Fig. 2. (a) SSIMC equivalent circuit with applied primary and secondary voltages. (b) SSIMC voltage and current components for a given switching cycle operating at $\theta$ within a sector.

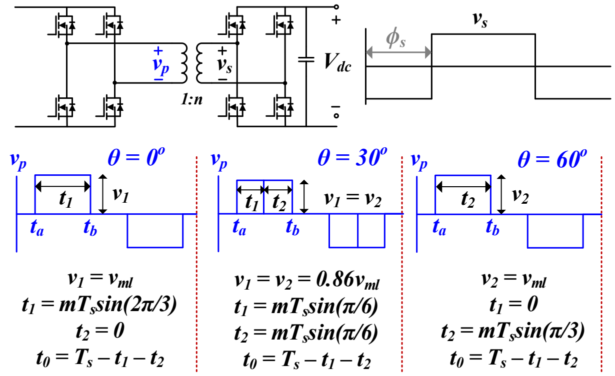


Fig. 3. Primary and secondary voltage patterns (at UPF) over a switching period ($T_s$), as $\theta$ varies from $0^o$ to $60^o$ in a sector.

showing the controllable power factor at the grid side. Similarly, [13] investigates the SSIMC for the inversion mode of operation with decoupled power control. The current literature on SSIMC validates the topology for a high-density, high-power DCFC system.

However, the current literature needs further investigation to study the SSIMC in reactive power compensation capability with qualitative analysis. The literature [8], [9], [10], and [11] mainly focuses on unity power factor operation. Whereas [12], and [13] discuss SSIMC with varied power factor operation, but the reactive power variation with different modes of operation is not considered. Hence, this paper analyzes the SSIMC, providing the variation of transformer primary voltage and the RMS current with the grid side power factor. Based on the results obtained, the SSIMC operation is considered in two modes of operation. Mode-I is defined with the battery in place while charging, and mode-II is where the SSIMC is idle with the output capacitor.

Thus, in section-II, the analytical model of SSIMC is discussed with analysis on transformer primary voltage, RMS current, grid active and reactive power variation with respect to grid side power factor. Consequently section-III shows the simulation results of SSIMC validating mode-I and II operation.

## II. SSIMC Power Flow Analysis

### A. Working Principle of SSIMC

The equivalent circuit of SSIMC can be represented as shown in Fig. 2(a), where the primary $(v_1, v_2)$ and secondary voltage $(v_s')$ components are represented using the superposition principle. Correspondingly, the current components $(i_1, i_2,$ and $i_s')$ due to the respective applied voltage are as shown. During a switching cycle $(T_s)$, the two line-to-line voltages with the highest magnitudes are selected as the primary voltage $(v_p)$ components, as shown in Fig.2(b). These selected voltages are then applied with calculated duty cycles to ensure that the average transformer voltage remains zero. This is achieved by applying the negative of the selected active vectors for equal durations. For this application, the secondary voltage is phase-shifted by 90° to the primary to achieve the maximum power transfer capability. The modulation implementation is as per [1] and [2].

### B. Modelling of SSIMC

The voltage components $(v_1, v_2)$ contributing to the primary voltage $(v_p)$ and the duty cycles $(t_1, t_2, t_0)$ at unity power factor (UPF) operation can be expressed as (1)-(2), where $v_{ml}$

$$v_1(\theta) = v_{ml}\cos(\theta),\, v_2(\theta) = v_{ml}\sin(\theta + \pi/6) \quad (1)$$

$$t_1(\theta) = mT_s\sin(\theta + 2\pi/3),\, t_2(\theta) = mT_s\sin(\theta)$$
$$t_0(\theta) = T_s - t_1(\theta) - t_2(\theta), m = \sqrt{i_{dref}^2 + i_{qref}^2} \quad (2)$$

is the line-to-line peak voltage of the grid supply, $m$ is the modulation index, $1/T_s$ is the switching frequency, $t_1, t_2$, and $t_0$ are the duration for which the active and zero switching states are applied, as shown in Fig. 2(b), and $\theta$ is the angle of the reference voltage vector within a given sector. It is seen that the primary voltage of DAB is a function of the modulation index and the reference vector position $(\theta)$in each sector. The primary voltage waveform at $\theta = 0^o, 30^o$ and $60^o$is shown in Fig. 3(b) with corresponding voltage components $(v_1, v_2)$ and duty cycles $(t_1, t_2, t_0)$. The secondary voltage $(v_s)$ is considered with a 50% duty cycle and 90° phase shift to the primary voltage.

Since the transformer RMS current, input and output power are nearly constant during a sector operation, the primary voltage at $\theta = 0^o, 30^o$ is considered as shown in Fig. 4. The expected transformer current follows a piecewise linear characteristic as shown in Fig 4. The duration of the linear segments normalized to the switching frequency are represented by $\alpha = \{\alpha_0, \alpha_1, \alpha_2, \alpha_3, \alpha_4, \alpha_5, \alpha_6\}$, where $\alpha$ is given by (3). The duration of each piecewise linear segment is

$$\alpha = (1/T_s)\{t_0/4, t_1/2, t_2/2, t_0/2, t_2/2, t_1/2, t_0/4\} \quad (3)$$

given by $\tau_k = \alpha_k T_s$, where $\sum_{k=0}^{6}\alpha_k = 1$ holds. For a given primary and secondary voltage, at $\theta = 0^o$, the nodes of the primary current waveform $(i_{p1}, i_{p2}, \dots i_{p7})$, as shown in Fig. 4, can be obtained as in Fig. 4. The piecewise linear representation of $i_p$ over a segment $k$ $(t_k$ to $t_{k+1})$, at $\theta = 0^o$ is given by (4), while (5) expresses the time-averaged DC offset of the node points. The analytical estimation of $i_p(\theta = 0^o)$ is obtained as

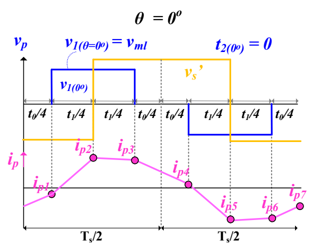


Fig. 4. SSIMC primary ($v_p$) and reflected secondary voltage ($v_s'$) waveforms with expected transformer primary current ($i_p$) shown at $\theta = 0^o$and $30^o$ in a sector operation.

$$i_{pk}(t) = i_{pk} + \frac{(i_{pk+1} - i_{pk})(t - t_k)}{\tau_k}, \quad t_k \leq t \leq t_{k+1}, 0 \leq k \leq 6, i_{po} = 0 \tag{4}$$

$$\overline{i_p} = (1/T_s) \sum_{k=0}^{k=6} \int_{t_k}^{t_{k+1}} i_{pk}(t)dt = \sum_{k=0}^{k=6} \alpha_k (i_k + i_{k+1})/2 \tag{5}$$

$$\widetilde{i_{pk}} = i_{pk} - \overline{i_p}, k = 0, \ldots, 7 \tag{6}$$

(6) by subtracting the time-averaged DC from the node points. Since the primary voltage waveform is similar at $\theta = 30^o$, the above methodology directly applies with corresponding values for primary voltage components and duty cycles.

The transformer RMS current can be estimated from the time-averaged node points by considering each linear segment separately. For a segment from $i_{pk}$ to $i_{pk+1}$, over a duration $\tau_k$ the RMS component is calculated using (7) and (8). Similarly,

$$\int_{t_k}^{t_{k+1}} i_{pk}(t)^2 dt = \tau_k (i_{pk}^2 + i_{pk} i_{pk+1} + i_{pk+1}^2)/3 \tag{7}$$

$$i_{prms} = \sqrt{\left(\frac{1}{3}\right) \sum_{k=0}^{k=6} \alpha_k (i_{pk}^2 + i_{pk} i_{pk+1} + i_{pk+1}^2)} \tag{8}$$

$$P = \left(\frac{1}{T_s}\right) \sum_{k \,\forall\, v_1 \neq 0} v_{1k} \left(i_{pk} + i_{pk+1}\right) \tau_k / 2 \tag{9}$$

the average output power from the primary side can be expressed as $P = 1/T_s \int_0^{T_s} v_p(t) i_p(t) dt$ as expressed in (9).

### C. *Effect of Grid Power Factor variation on Primary Voltage, Transformer RMS Current, Output Power, and Grid Reactive Power*

At an arbitrary grid power factor angle ($\phi$), the reference vector is generated at an angle of $\delta = \phi - \pi/6$, in the *d-q* plane, where the length of the reference vector represents the modulation index ($m$). Accordingly, the primary voltage components ($v_1, v_2$) at an operating point ($\theta$) in a sector follows (10), which is a function of power factor angle.

$$v_1(\theta) = v_{ml} \sin(\theta + \pi/3 - \delta), \quad v_2(\theta) = v_{ml} \sin(\theta - \delta) \tag{10}$$

Similarly, at $\theta = 0^o$(operating point in the sector), the primary

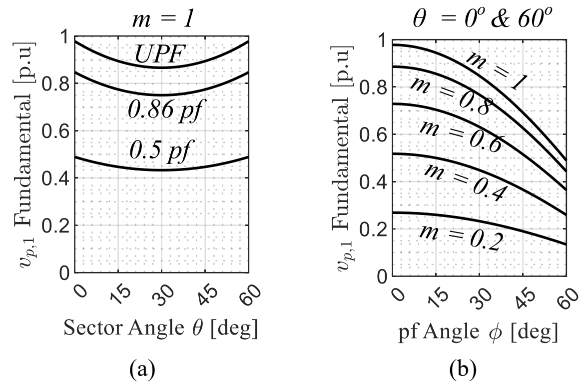


Fig. 5. Primary fundamental voltage ($\widetilde{v_{p,1}}$) variation shown (a) within a sector operation and (b) with variation in grid power factor ($\phi$) and modulation index ($m$).

fundamental voltage component is given by $\left(\frac{4v_1}{\pi}\right) \sin\left(\frac{m\pi t_1}{4}\right)$, which is a function of the modulation index ($m$). Using these relations, the variation of primary voltage components ($v_1, v_2$) and the fundamental component $\widetilde{v_{p,1}}$ at other grid power factors can be calculated. Since the primary voltage waveform is similar at other operating points in a sector, the overall primary fundamental voltage follows $\widetilde{v_{p,1}}$ as shown in Fig. 5. As the grid power factor angle increases up to 90°, the primary fundamental voltage decreases depending on the modulation index as shown in Fig. 5(b).

A similar analysis of transformer RMS current with grid power factor varying between UPF to ZPF, and modulation index varying from 0.2 to 1, is shown in Fig. 6(a). In this study, the secondary voltage is maintained at its rated value. Though the primary fundamental voltage is zero at ZPF, the transformer RMS current is maintained at 0.75 p.u due to the secondary voltage, as shown in Fig. 6(a). Correspondingly, the primary to secondary average power variation is shown in Fig. 6(b). It is seen that the peak grid current always occurs at the instant of $\theta = 0^0$, as shown in Fig. 3(b), since only one line-to-line voltage is utilized for primary voltage, during the switching period. Thus, the peak grid current can be estimated using (11).

$$i_{ml} = \left(\frac{1}{T_s}\right) \sum_{k \,\forall\, v_1 \neq 0} \left(i_{pk} + i_{pk+1}\right) \tau_k / 2 \tag{11}$$

Correspondingly, the obtained peak grid current and reactive power, as the modulation index varied from 0.2 to 1, and the power factor varied from UPF to ZPF, are shown in Fig. 6(c) and Fig. 6(d), respectively. The grid peak current is seen to be constant for a given modulation index ($m$), irrespective of the power factor angle, as shown in Fig. 6(c). The variation of grid peak current with respect to the transformer RMS current is shown in Fig. 7, where the secondary voltage is maintained at the rated value.

### D. *Control implementation of the SSIMC system*

The reference signals $V_{dc}^*$ and $i_{qref}$ are applied depending on the desired output DC voltage and the grid-side reactive power, as shown in Fig. 8. The conventional d-q current controllers are directly applicable to the SSIMC system, as used in VSI

979-8-3315-8138-1

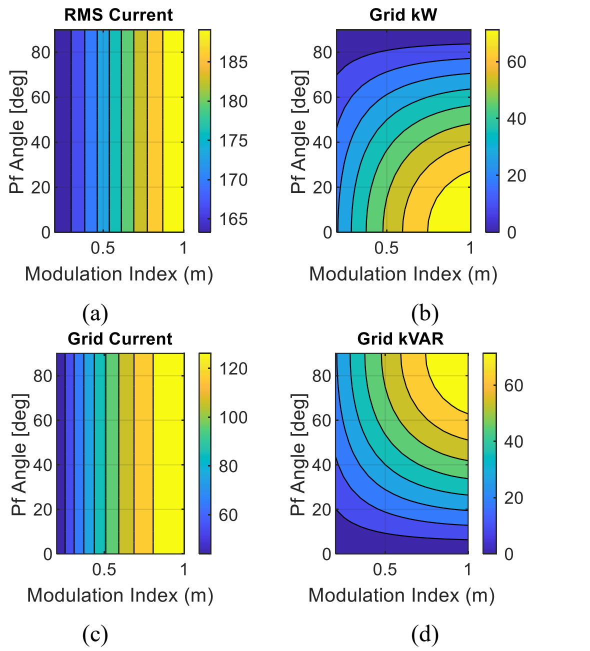


Fig. 6. Variation of (a) transformer RMS current, (b) primary to secondary output power, (c) grid peak current, and (d) reactive power at the grid, as $m$ varies from 0.2 to 1 and power factor varies from UPF to ZPF.

converters due to the implemented modulation methodology as discussed in [14]. This inherently simplifies the control structure, similar to a grid-connected VSI. The control structure remains the same with mode-II operation, where only the output capacitor is present without the battery. The d-axis reference component is accordingly lowered just enough to maintain a constant voltage across the capacitor, as implemented in a conventional STATCOM application.

## III. Simulation Results

The simulation is conducted in PLECS software for an SSIMC system with a 60-kW power rating, three-phase 480 V AC input, and 800 V DC output. The simulation parameters are provided in Table I. The leakage inductance and the isolation transformer turn ratio are set to match the 800 V DC output voltage and the desired power rating of the converter. The following sections present the simulation results.

The reactive power variation in mode-I operation with varied battery voltage is shown in Fig. 9(a), with three cases such as (A), (B), and (C). The output voltage varies from 400 V, 600 V, and 800 V, respectively, with a constant modulation index $m = 0.8$, at the primary side with a constant power factor of 0.707 pf leading maintained at the grid. The obtained primary RMS current and the reactive power at these three conditions (A), (B), and (C) are 100A, 30 kVAR, 140A, 40 kVAR, and 180A, 60 kVAR, respectively, as shown in Fig. 9(a). At a given battery voltage, the maximum reactive power support to the grid is varied, and it is maximum when the battery voltage is at the rated value. It is seen that the charging current is maintained while supporting the grid in the above conditions. The mode-II operation, where the capacitor voltage is maintained at 800 V

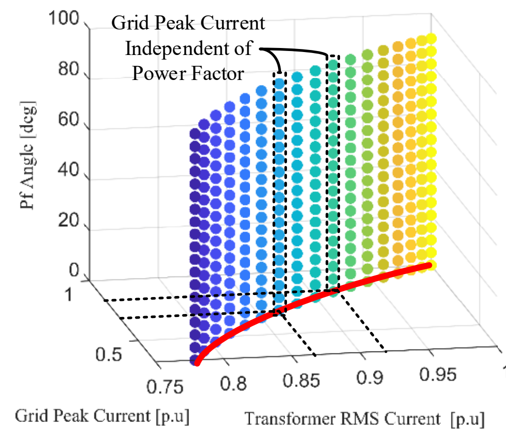


Fig. 7. Variation of transformer RMS current and grid peak current, as $m$ varies from 0.2 to 1 and power factor varies from UPF to ZPF.

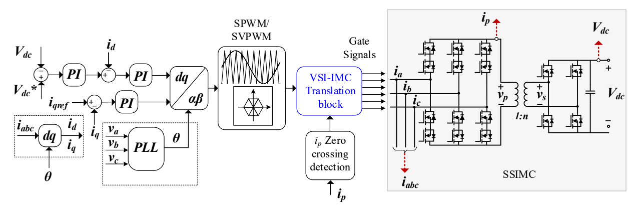


Fig. 8 Output voltage and power control methodology.

TABLE I. Simulation Parameters of 60 kW SSIMC.

| Parameter | Value |
|---|---|
| Grid Voltage | 480 $V_{rms}$, 60 Hz |
| Output Power, $S_n$ | 60 kW |
| Voltage Output, $V_O$ | 800 V |
| SiC Device Part Number | C3M0021120K |
| Leakage Inductance | 18 µH |

while supplying the maximum rated reactive power (70 kVAR) to the grid, is shown in Fig. 9(b). The power factor in this mode is maintained at 90° leading, as in the case of a capacitor-based reactive power compensation.

## V. Conclusion

In conclusion, this paper presented a comprehensive analytical investigation of the single-stage indirect matrix converter (SSIMC) for DC fast charger (DCFC) applications, focusing on its capability to support reactive power compensation in addition to bidirectional active power transfer. The developed analytical model established the relationships between modulation index, power factor angle, and resulting active and reactive power characteristics of the SSIMC. Two distinct operational modes were defined—mode-I, representing G2V operation with the battery connected, and mode-II, representing the idle condition with an output capacitor replacing the battery. The analysis demonstrated that during mode-II, the SSIMC can effectively operate as a reactive power compensator at its rated capacity, thereby providing ancillary grid support without additional hardware. The study revealed the impact of grid power factor variation on transformer RMS

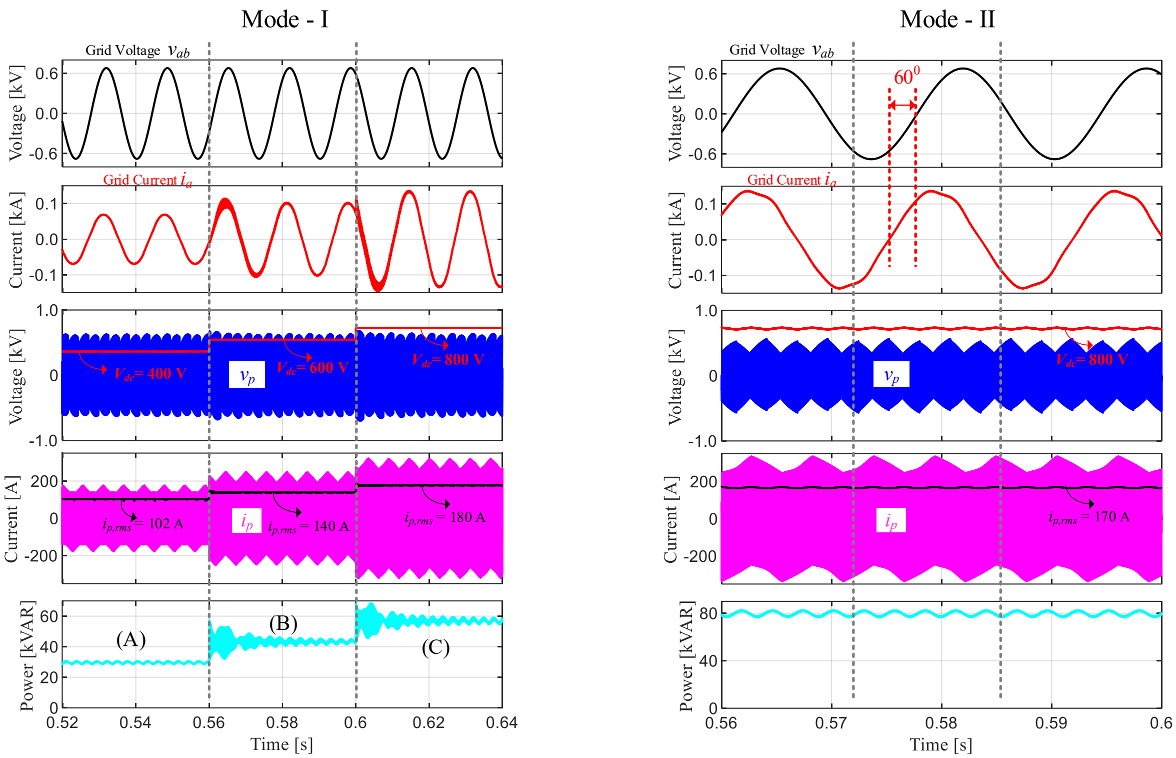


(a) (b)

Fig. 9. Simulation results showing SSIMC operation (a) mode-I operation with varying battery voltage, and (b) mode-II operation with voltage-controlled DC capacitor.

current and power transfer characteristics. The proposed analytical framework and results serve as a foundation for optimized control and design of SSIMC-based EV chargers, enabling their integration as multifunctional grid-interactive converters in future smart grid infrastructures.

## REFERENCES

[1] M. Benson, A. Dornala, M. Andleeb, K. Lee, and W. Lee, "Simple and Robust Carrier-Based PWM Technique for Single-Stage Three-phase Rectifier Indirect Matrix Converter, "*2024 IEEE Applied Power Electron. Conf. and Expo., (APEC)*, Long Beach, CA, USA, 2024.

[2] A. Dornala and W. Lee, "Optimal Modulation Methodology for Efficient Operation of Single-Stage Indirect Matrix Converter," *2025 IEEE/AIAA Transportation Electrification Conference and Electric Aircraft Technologies Symposium (ITEC+EATS)*, Anaheim, CA, USA, 2025.

[3] M. C. Kisacikoglu, M. Kesler and L. M. Tolbert, "Single-Phase On-Board Bidirectional PEV Charger for V2G Reactive Power Operation," in *IEEE Trans. on Smart Grid*, vol. 6, no. 2, pp. 767-775, March 2015,

[4] M. C. Kisacikoglu, B. Ozpineci, and L. M. Tolbert, "EV/PHEV Bidirectional Charger Assessment for V2G Reactive Power Operation," in *IEEE Trans. on Power Electron.*, vol. 28, no. 12, pp. 5717-5727, Dec. 2013,

[5] D. B. Wickramasinghe Abeywardana, P. Acuna, B. Hredzak, R. P. Aguilera, and V. G. Agelidis, "Single-Phase Boost Inverter-Based Electric Vehicle Charger With Integrated Vehicle to Grid Reactive Power Compensation," in *IEEE Trans. Pow. Electron.*, vol. 33, no. 4, pp. 3462-3471, April 2018.

[6] H. Tanaka, F. Ikeda, T. Tanaka, H. Yamada and M. Okamoto, "Novel Reactive Power Control Strategy Based on Constant DC-Capacitor Voltage Control for Reducing the Capacity of Smart Charger for Electric Vehicles on Single-Phase Three-Wire Distribution Feeders," in *IEEE Journal of Emerging and Selected Topics in Power Electronics*, vol. 4, no. 2, pp. 481-488, June 2016.

[7] M. Nikkhah Mojdehi and P. Ghosh, "An On-Demand Compensation Function for an EV as a Reactive Power Service Provider," in *IEEE Transactions on Vehicular Technology*, vol. 65, no. 6, pp. 4572-4583, June 2016.

[8] N. Weise, K. Basu and N. Mohan, "Advanced modulation strategy for a three-phase ac-dc dual active bridge for v2g",Proc. *IEEE Veh. Power Propulsion Conf.*, pp. 1-6, 2011.

[9] L. Schrittwieser, M. Leibl and J. W. Kolar, "99% efficient isolated three-phase matrix-type DAB buck–boost PFC rectifier", *IEEE Trans. Power Electron.*, vol. 35, no. 1, pp. 138-157, Jan. 2020.

[10] N. R. Mirković, Đ. M. Stojić, A. Delgado, P. Alou, and M. Vasić, "Novel Three-Phase to Single-Phase Matrix Converter Modulation Strategy for Bidirectional Inductive Power Transfer," in *IEEE Trans. on Power Electron.*, vol. 38, no. 12, pp. 14830-14846, Dec. 2023.

[11] J. Afsharian, D. D. Xu, B. Gong and Z. Yang, "Space vector demonstration and analysis of zero-voltage switching transitions in three-phase isolated PWM rectifier", *Proc. IEEE Energy Convers. Congr. Expo.*, pp. 2477-2484, 2015.

[12] Varajão, R. E. Araújo, L. M. Miranda and J. A. P. Lopes, "Modulation strategy for a single-stage bidirectional and isolated AC–DC matrix converter for energy storage systems", *IEEE Trans. Ind. Electron.*, vol. 65, no. 4, pp. 3458-3468, Apr. 2018.

[13] K. Shigeuchi, J. Xu, N. Shimosato, and Y. Sato, "A modulation method to realize sinusoidal line current for bidirectional isolated three-phase AC/DC dual-active-bridge converter based on matrix converter", *IEEE Trans. Power Electron.*, vol. 36, no. 5, pp. 6015-6029, May 2021.

[14] A. Dornala, M. Benson and W. Lee, "A Translation-Based Modulation for Single-Stage Three-phase Rectifier Indirect Matrix Converter," in *IEEE Trans. on Power Electronics*, doi: 10.1109/TPEL.2026.3660800.

979-8-3315-8138-1